ACS NANO
Cite This: ACS Nano 2017, 11, 12482–12491
www.acsnano.org

ARTICLE

Intrabilayer ^{64}Cu Labeling of Photoactivatable, Doxorubicin-Loaded Stealth Liposomes

Dandan Luo,[†] Shreya Goel,[‡] Hai-Jun Liu,[§] Kevin A. Carter,[†] Dawei Jiang,[∥] Jumin Geng,[†] Christopher J. Kutyreff,[⊥] Jonathan W. Engle,[⊥] Wei-Chiao Huang, Shuai Shao,[†] Chao Fang,[*,§] Weibo Cai,[*,‡,∥,⊥,#] and Jonathan F. Lovell[*,†]

[†]Department of Biomedical Engineering, University at Buffalo, State University of New York, Buffalo, New York 14260, United States
[‡]Department of Materials Science and Engineering, [∥]Department of Radiology, [⊥]Department of Medical Physics, and [#]University of Wisconsin Carbone Cancer Center, University of Wisconsin—Madison, Madison, Wisconsin 53705, United States
[§]Hongqiao International Institute of Medicine, Shanghai Tongren Hospital and Department of Pharmacology, Institute of Medical Sciences, Shanghai Jiao Tong University School of Medicine (SJTU-SM), 280 South Chongqing Road, Shanghai 200025, China

Supporting Information

ABSTRACT: **Doxorubicin (Dox)-loaded stealth liposomes (similar to those in clinical use) can incorporate small amounts of porphyrin−phospholipid (PoP) to enable chemophototherapy (CPT). PoP is also an intrinsic and intrabilayer ^{64}Cu chelator, although how radiolabeling impacts drug delivery has not yet been assessed. Here, we show that ^{64}Cu can radiolabel the stable bilayer of preformed Dox-loaded PoP liposomes with inclusion of 1% ethanol without inducing drug leakage. Dox-PoP liposomes labeled with intrabilayer copper behaved nearly identically to unlabeled ones *in vitro* and *in vivo* with respect to physical parameters, pharmacokinetics, and CPT efficacy. Positron emission tomography and near-infrared fluorescence imaging visualized orthotopic mammary tumors in mice with passive liposome accumulation following administration. A single CPT treatment with 665 nm light (200 J/cm^2) strongly inhibited primary tumor growth. Liposomes accumulated in lung metastases, based on NIR imaging. These results establish the feasibility of CPT interventions guided by intrinsic multimodal imaging of Dox-loaded stealth PoP liposomes.**

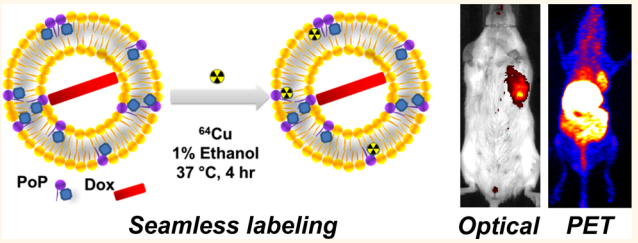

KEYWORDS: *liposomes, porphyrin−phospholipid, doxorubicin, image-guided drug delivery, chemophototherapy*

Nanomaterials integrating multiple functionalities can be used in the emerging biomedical field of image-guided drug delivery (IGDD).[1−5] Numerous organic and inorganic nanoparticles hold potential for IGDD.[6−13] Liposomes are a common organic drug delivery vehicle and have also been explored for this purpose.[14−16] For example, thermal-responsive liposomes loaded with doxorubicin (Dox) and a magnetic resonance contrast agent can be used in combination with heat to ablate tumors while simultaneously ascertaining local drug distribution.[17]

Beyond predicting delivered drug concentrations, IGDD could be useful for image-guided interventions. Our group developed light-activated, doxorubicin-loaded, porphyrin−phospholipid (PoP) liposomes for use as a single-agent antitumor treatment using chemophototherapy (CPT).[18−20] PoP itself confers capabilities for seamless and intrinsic imaging using positron emission tomography (PET) and fluorescence. Imaging of PoP liposomes could be used to demark metastatic tumor locations using a whole body technique such as PET, which is extensively used in clinical oncology.[21] Once tumors are roughly identified, multiple narrow fiber optic cables could be inserted into tumor sites with additional guidance from the near-infrared (NIR) fluorescence of PoP. Interstitial treatment with such image guided planning represents a minimally invasive method to treat tumors of any size in the body.[22]

Several strategies have been proposed for generating bioresponsive materials and improving liposomal drug delivery.[23,24] Many light-triggered release approaches have been developed.[25−27] We recently reported long-circulating doxorubicin in PoP liposomes capable of NIR light-triggered drug release.[28] This is of note since long-circulating sterically stabilized liposomal Dox (SSLD) is already used for treating several cancer types.[29] It was shown to be noninferior and less toxic than the free drug in treating breast cancer and is used off label for that indication.[30] Therefore, a long-term vision could be that (1) patients with metastatic disease could receive a single PoP liposome chemotherapy agent consistent with

Received: September 16, 2017
Accepted: December 1, 2017
Published: December 1, 2017

DOI: 10.1021/acsnano.7b06578
ACS Nano 2017, 11, 12482−12491

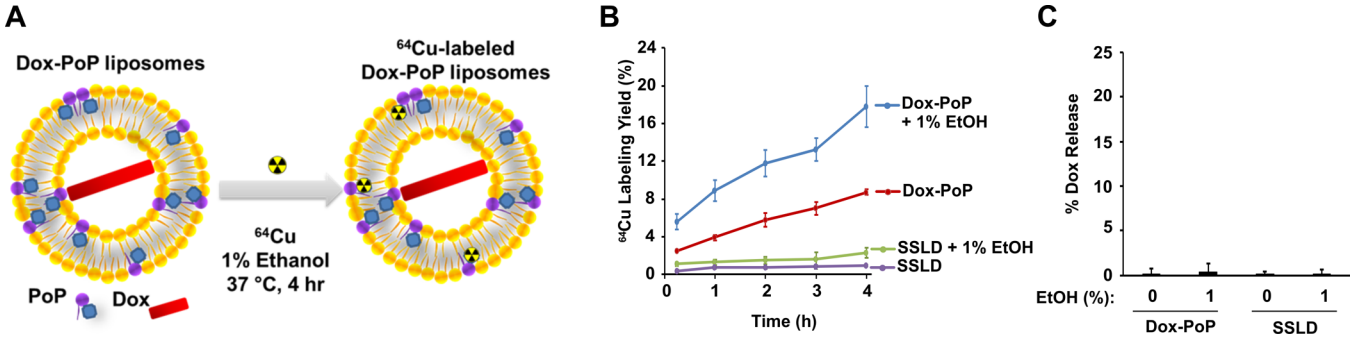

Figure 1. ^{64}Cu labeling of Dox-PoP liposomes. (A) Generation of Dox-loaded CuPoP liposomes. (B) Time-dependent ^{64}Cu labeling of Dox-PoP liposomes and sterically stabilized liposomal Dox (SSLD) in 0.1 M sodium acetate buffer (pH 5.5) at 37 °C with or without the addition of 1% ethanol (v/v) in the labeling solution. (C) Dox leakage from liposomes following the labeling incubation. Data represent mean ± SD for n = 3.

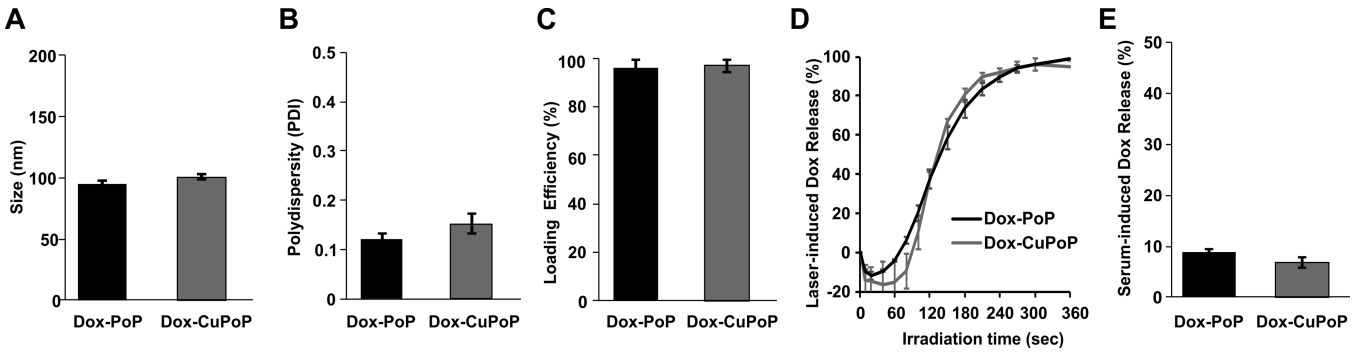

Figure 2. Characterization of Dox-PoP and Dox-CuPoP liposomes. (A) Size of Dox-PoP and Dox-PoP liposomes following labeling with Cu (CuPoP liposomes). (B) Polydispersity of Dox-PoP and Dox-CuPoP liposomes. (C) Loading efficiency of Dox-PoP and Dox-CuPoP liposomes. (D) Dox release in 50% serum at 37 °C upon 665 nm laser irradiation (250 mW/cm^2). (E) Serum-induced Dox leakage of Dox-PoP and Dox-CuPoP liposomes following incubation in 50% adult bovine serum at 37 °C for 6 h. Mean ± SD for n = 3.

standard of care treatment; (2) 24 h after drug administration, PET could be used to identify large metastatic tumor sites where liposomes accumulated; and (3) PoP NIR fluorescence is used to guide optical fiber placement in the tumors for potent tumor photoablation. In theory, imaging could also estimate local drug concentrations which in turn could guide light dosimetry. This approach represents an IGDD paradigm to simultaneously treat local disease and metastatic disease in advanced cancer patients.

Traditionally, liposomes have been successfully used for whole body imaging techniques by modification of liposome formulations to include radionuclide chelators covalently linked to lipids.[31] The radionuclide is then mixed with the liposomes. Several recent approaches for radionuclide nanoparticle labeling involve chelator-free approaches.[32−36] For liposomes, to avoid having to modify the lipid composition of the formulation, other approaches have been reported in which copper and other radionuclides are actively loaded inside the liposomes.[37−39] PoP can be chelated with various divalent cationic metals such as copper within the hydrophobic portion of bilayer.[40−43] PoP-based nanoparticles such as lipoprotein-mimicking nanoparticles have been used for seamless PET labeling and imaging combined with photodynamic therapy in clinically relevant preclinical cancer models.[44] One-pot copper labeling of nearly pure PoP itself has been reported with a 95% labeling yield in just 30 min.[45] Despite these promising results, as indicated by the ready metal ion access to the porphyrin, such structures likely would not be appropriate for carrying and delivering cargo in stably enclosed liposome volumes. It is not known if stable, cargo-loaded liposomes can be labeled with ^{64}Cu without inducing drug leakage. Here, we demonstrate copper labeling of stable bilayers of stealth liposomes that include a small amount of PoP.

RESULTS AND DISCUSSION

Ethanol Enhances ^{64}Cu-Labeling of Sterically Stabilized PoP Liposomes. We previously showed that PoP can chelate metals (e.g., Zn, Cu, Ni, Co) and then form liposomes.[40−43] However, those approaches involve direct metal labeling of PoP in organic solvent, purification, and downstream liposome formation. When hydrated, PoP bilayers themselves are hydrophobic with limited access to aqueous solvent.[46] This poses a challenge for the goal of intrabilayer labeling of preformed, drug-loaded liposomes (Figure 1A).

The stealth Dox-PoP liposomes included distearoylphosphatidylcholine (DSPC), PoP, cholesterol (CHOL), and a polyethylene glycol lipid (DSPE-2000-PEG); [DSPC/PoP/cholesterol/DSPE-2000-PEG], [53:2:40:5], mol % at the drug to lipid ratio of 1:6 and were prepared by ethanol injection followed by extrusion as previously described.[28] When Dox-PoP liposomes were incubated with $^{64}CuCl_2$, limited labeling efficiency was observed, only ∼8% after a 4 h incubation. We assessed whether ethanol, which is used during liposome formation (prior to removal with dialysis) and is known to impact bilayer behavior, could enhance labeling yields. Ethanol (1%) was able to double the labeling efficiency (Figure 1B). Addition of ethanol from 1% to 10% did not induce any obvious leakage of Dox during the labeling process itself

DOI: 10.1021/acsnano.7b06578
ACS Nano 2017, 11, 12482−12491

(Figure 1C and Figure S1). Ethanol has been reported to interact strongly with phosphatidylcholine bilayers and induce alteration of the headgroups and disordering of lipid side chains.[47] This presumably enables the divalent copper cation, which bilayers are normally impermeable to, to better access the porphyrin side chain and become chelated.

Effect of Copper Labeling on Dox-PoP Liposomes. The properties of Dox-PoP liposomes were assessed following cold copper labeling. On the basis of cryogenic transmission electron microscopy, the morphology of Dox-PoP liposomes appeared as 100 nm, slightly elongated unilamellar vesicles that entrapped fibrous Dox precipitations in the aqueous core of the liposomes (Figure S2A). On the basis of light-scattering, the size of Cu-labeled Dox-PoP liposomes (Dox-CuPoP liposomes) and the original Dox-PoP liposomes was 101 and 96 nm, respectively (Figure 2A). The polydispersity index of labeled and unlabeled Dox-PoP liposomes was 0.15 and 0.12, respectively (Figure 2B). Both labeled and unlabeled liposomes exhibited over 98% drug loading efficiency (Figure 2C), confirming no drug leakage during the labeling process. The NIR light triggered-release profile with a 665 nm laser diode at 250 mW/cm^2 is shown in Figure 2D, with 90% Dox release occurring in 4 min for both types of liposomes. After laser treatment, the size of Dox-CuPoP liposomes decreased slightly to 94 nm, without significant change to the polydispersity index (Figures S2B and S2C). We have previously shown that light-induced Dox release is likely due to PoP-mediated photo-oxidation of unsaturated lipids (such as cholesterol) which transiently disrupt the lipid bilayer to induce release of actively or passively loaded cargo.[48,49] At a lower fluence rate (100 mW/cm^2), laser-induced Dox release rate was slower, with 90% drug release in 9.3 min (Figure S3A). This is likely due to the lower amount singlet oxygen generation at the lower fluence rate (Figure S3B). Dox leakage during serum incubation at 37 °C for 6 h was less than 10% for both Dox-CuPoP liposomes and Dox-PoP liposomes (Figure 2E). Taken together, copper-labeled liposomes behaved similarly to Dox-PoP liposomes *in vitro*, implying labeling conditions and the presence of copper in the bilayer had minimal impact on bilayer stability or light-triggered release.

Pharmacokinetics (PK). To verify whether copper labeling modified the *in vivo* behavior of the liposomes, PK of labeled liposomes and unlabeled Dox-PoP liposomes was compared. Following intravenous injection of 7 mg/kg Dox-loaded liposomes to ICR mice, serum was collected at the indicated time points. As shown in Figure 3 and Table 1, both Dox-CuPoP and Dox-PoP liposomes exhibited long circulation half-lives (18.5 h vs 15.1 h). Dox-CuPoP liposomes showed slightly lower Cmax (158.1 vs126.8 μg/mL) and a slight decrease (10.1%) of AUC$_{last}$, suggesting perhaps that a small fraction of Dox leaked during circulation. Overall, Dox-CuPoP liposomes demonstrated satisfactory *in vivo* stability, similar to Dox-PoP liposomes.

PET Imaging of Dox-CuPoP Liposomes. Female BALB/c mice bearing orthotopic 4T1 mammary tumors were intravenously injected with 7 mg/kg of Dox-^{64}CuPoP liposomes. With PET, the tumor area could clearly be visualized (Figure 4A). Tumor uptake of liposomes is based on passive accumulation due to the enhanced permeability and retention effect.[50] Quantitative, imaging-based, kinetic distribution of liposomes in tumors and main organs is shown in Figure 4B. The amount of liposomes in the tumor increased to 5.3 % injected dose per gram (% ID/g) from 0.5 to 24 h. A large amount of liposomes accumulated in the liver and spleen, as the main organs of the reticuloendothelial system. The amount of liposomes in liver reached a maximum amount by 3 h (38.1 % ID/g) and slightly decreased to 29.1 % ID/g by 24 h. Mice were sacrificed at the 24 h time point and biodistribution of liposomes in each organ was quantified by gamma counting (Figure 4C). *Ex vivo* biodistribution was in accordance with the *in vivo* imaging-based measurements, with the highest amount of Dox-CuPoP liposomes accumulating in the liver (24.9 % ID/g). The amount of liposomes in the tumor was 3.6 % ID/g by *ex vivo* measurement.

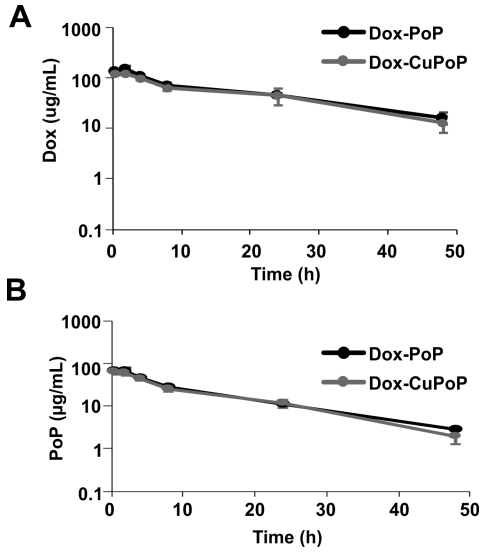

Figure 3. Pharmacokinetics of Dox-CuPoP and Dox-PoP liposomes. ICR Mice were intravenously injected with 7 mg/kg liposomal Dox. Dox (A) and PoP (B) serum concentrations were measured for the indicated liposomes. Mean ± SD for n = 4.

Table 1. Noncompartmental Analysis of Dox-CuPoP Liposome and Dox-PoP Liposome PK

parameter	Dox-PoP	Dox-CuPoP
$T_{1/2}$ (h)	18.5	15.1
T_{max} (h)	2	2
C_{max} (μg/mL)	158	127
AUC$_{last}$ (μg/mL·h)	2552	2294
AUC$_{(0\text{-inf})}$ (μg/mL·h)	2992	2576
CL (mL/h/g)	0.0035	0.004
V_{ss} (mL/g)	0.06	0.06

NIR Fluorescence Imaging of Dox-CuPoP. While PET is a whole body technique, NIR fluorescence could be complementary for assessing local accumulation of liposomes. For example, PET could be used for rough approximation of tumor location, and fluorescence could be used to pinpoint the tumor sites using fiber optic probes for phototherapy. Mice were also subjected to NIR fluorescence imaging. Although copper quenches PoP fluorescence, only a small fraction of the PoP is labeled by ^{64}C. Approximately 90% of the NIR fluorescence emission of the liposomes was retained following the labeling procedure (Figure S3C). As shown in Figure 5A, tumor regions were clearly identified by NIR fluorescence. The signal in tumors showed a slight increase after 0.5 h, further increasing over 24 h (Figure 5B). This coincides with the PET data in Figure 4B. *Ex vivo* imaging of the tumor, main organs (liver, kidney, spleen, heart, lung), and tissues (skin and

DOI: 10.1021/acsnano.7b06578
ACS Nano 2017, 11, 12482−12491

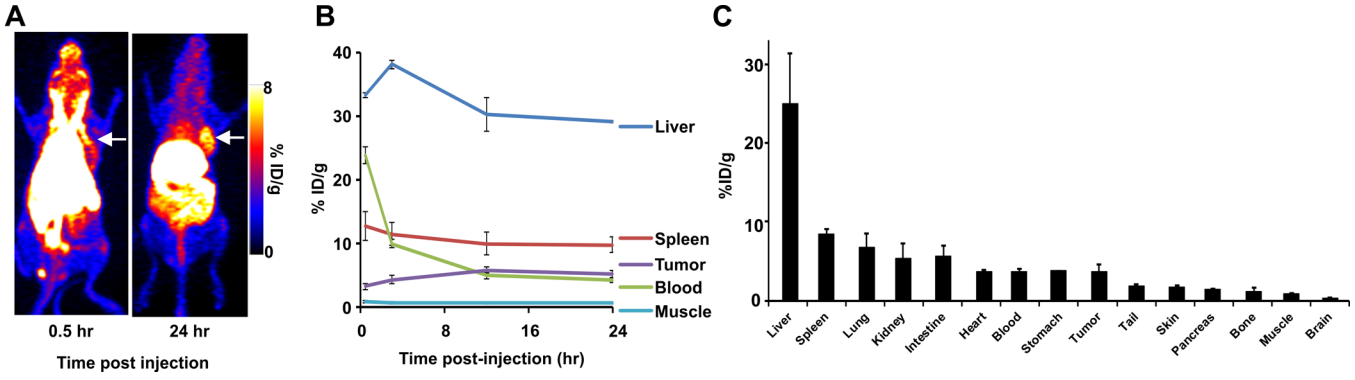

Figure 4. *In Vivo* PET imaging and biodistribution of Dox-CuPoP. Mice bearing orthotopic 4T1 mammary tumors were intravenously injected with 7 mg/kg Dox-^{64}CuPoP liposomes. (A) PET scan of mice following Dox-CuPoP administration. Tumor location is indicated by the white arrow. (B) Quantitative imaging-based accumulation kinetics of liposomes in tumor and other organs. (C) Biodistribution of liposomes in extracted organs 24 h post administration based on gamma counting. Data are shown as mean ± SD for n = 3.

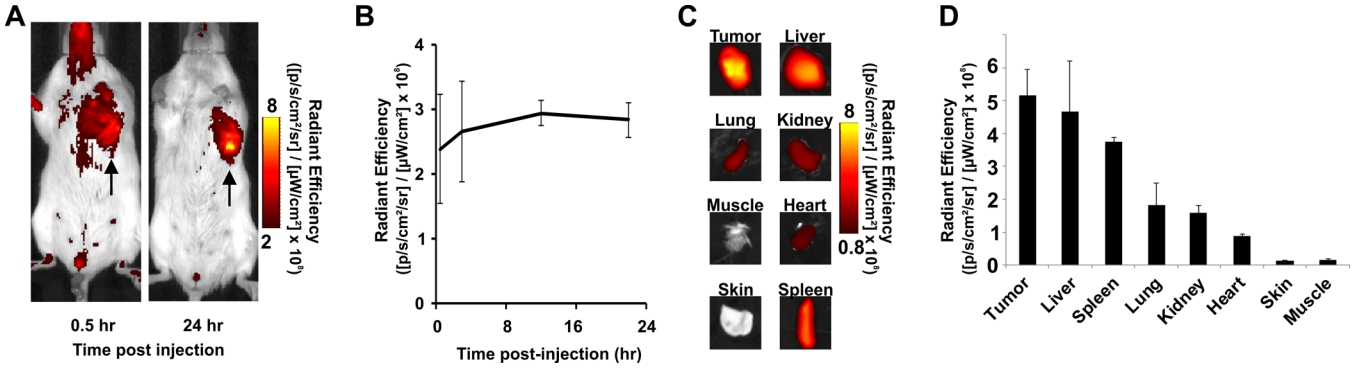

Figure 5. NIR fluorescence imaging using Dox-CuPoP. Mice bearing orthotopic 4T1 mammary tumors were intravenously injected with 7 mg/kg of Dox-CuPoP liposomes. (A) NIR fluorescence imaging of mice after administration of Dox-CuPoP liposomes. (B) *In vivo* tumor NIR imaging signal of Dox-CuPoP liposomes. (C) *Ex vivo* imaging of tumor and main organs. (D) Quantitative fluorescence signal in tumor and main organs and tissue. Data represent mean ± SD for n = 3.

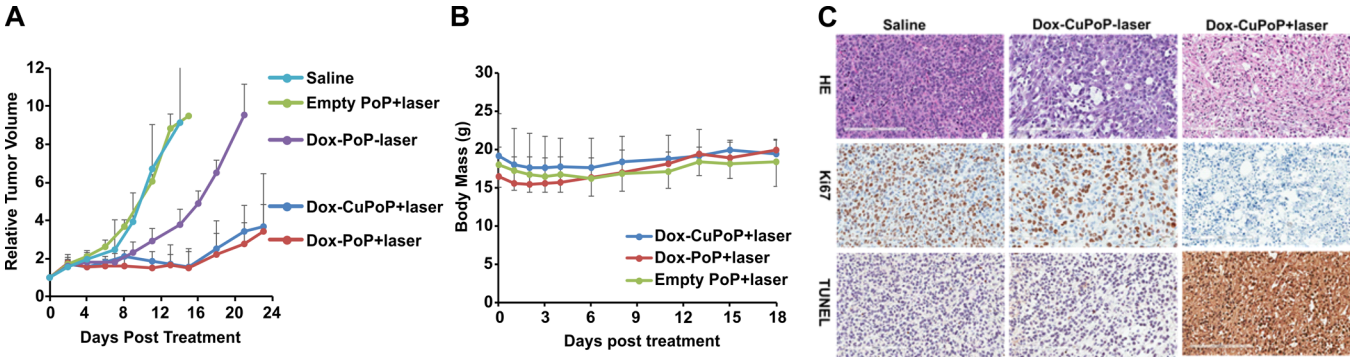

Figure 6. Chemophototherapy using Dox-Cu-PoP in mice bearing orthotopic 4T1 tumors. (A) Relative tumor growth in treated mice. Mice were intravenously injected with liposomes (7 mg/kg Dox) or empty PoP liposomes (equivalent to 7 mg/kg Dox). Three groups received laser treatment (200 J/cm^2; 100 mW/cm^2 for 33.3 min) 24 h post drug administration. (B) Body weights of mice following treatments. Data represent mean ± SD for n = 6. (C) HE, Ki67 and TUNEL staining of tumor slices from mice receiving indicated treatments (same conditions as in tumor growth study). Tumors were collected 72 h after drug administration (48 h after laser treatment). A scale bar of 200 μm is shown.

muscle) showed a high fluorescence signal in liver, spleen, and tumor (Figure 5C). Quantification of fluorescence imaging is shown in Figure 5D, with the highest fluorescence being observed in the tumor. This result is different from the ^{64}Cu biodistribution, which may be due to differing optical properties of the various organs examined, or differences in intratissue liposome localization. In general, fluorescence imaging of organs and tissues is not as reliable a method for biodistribution calculation compared to gamma counting or tissue extraction techniques.

Chemophototherapy Using Dox-CuPoP. The efficacy of Dox-CuPoP liposomes was compared to Dox-PoP liposomes in the same breast cancer mouse model used for imaging studies. Mice bearing orthotopic 4T1 tumors were intravenously administered 7 mg/kg of Dox-CuPoP or Dox-PoP liposomes, empty PoP liposomes, or saline. Twenty-four hours after intravenous injection, tumors were irradiated with 665 nm light

DOI: 10.1021/acsnano.7b06578
ACS Nano 2017, 11, 12482−12491

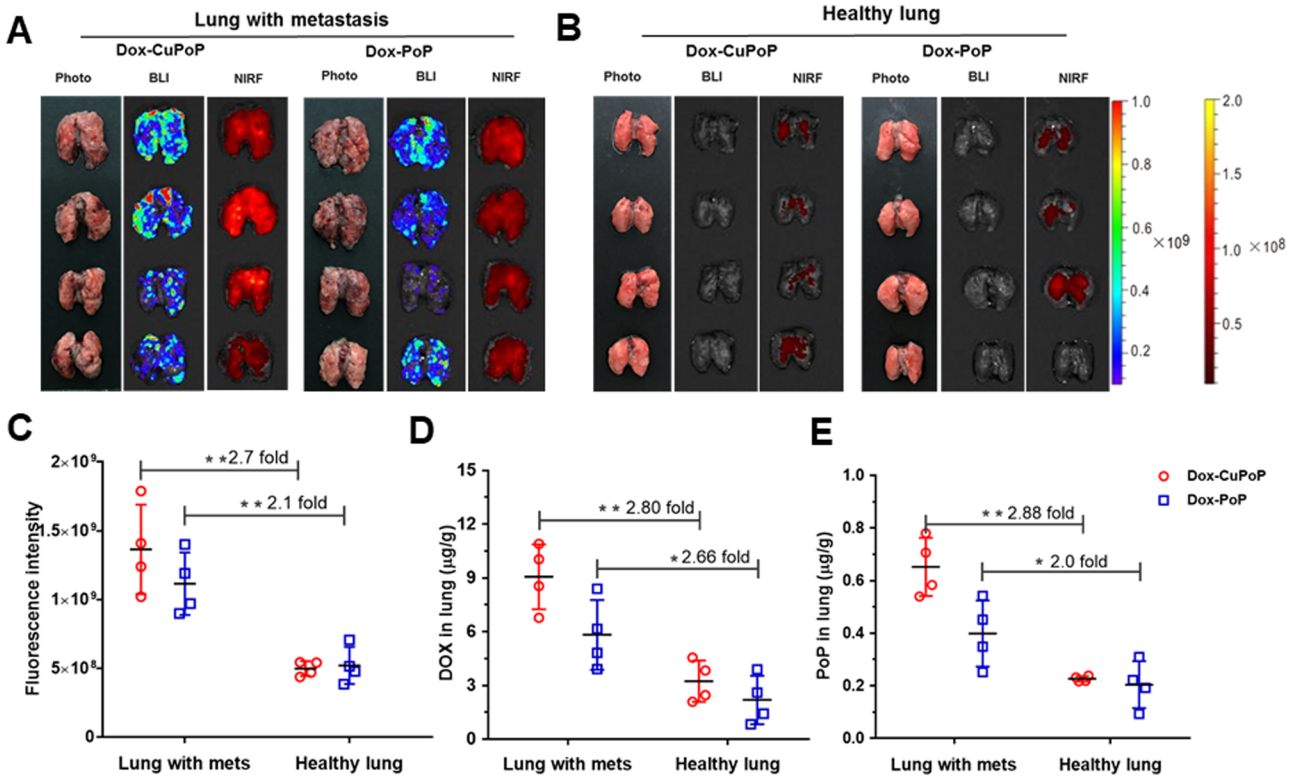

Figure 7. Macroscopic NIR imaging of Dox-CuPoP accumulation in 4T1 lung metastases. Mice were intravenously administered with 5 mg/kg Dox-CuPoP liposomes or Dox-PoP liposomes. *Ex vivo* image through bioluminescence and NIR fluorescence (NIRF) for PoP (Exc: 657 nm, Em: 720 nm) for lungs with metastasis (A) or healthy lungs (B) 24 h following Dox-CuPoP and Dox-PoP (5 mg/kg Dox) intravenously administration. (C) PoP fluorescence intensity in the lungs with metastasis and healthy lungs. (D) Dox and (E) PoP concentrations in lung homogenates with or without metastasis. Data represent mean ± SD for $n = 4$.

(200 J/cm^2). This time point was selected since it would theoretically enable PET imaging to be carried out to first identify tumor sites to be treated with phototherapy. Some swelling in the treated tumor region was observed following laser treatment. As shown in Figure 6A, Dox-CuPoP liposomes and Dox-PoP liposomes induced very similar antitumor efficacy, with tumor growth strongly inhibited for 2 weeks. Five out of six mice (83.3% survival rate) from both groups avoided the tumor growth end point (10 times of initial volume) by day 21. Both Dox-CuPoP liposomes and Dox-PoP liposomes with laser treatment were more effective than Dox-PoP liposomes alone (***$p < 0.0001$, student's t test). Without laser treatment, five out of six mice reached the tumor growth end point by day 21, for a survival rate of just 16.7%. Dox-PoP liposomes without laser treatment inhibited tumor growth compared to the saline control group (**$p = 0.0026$, student's t test). Empty PoP liposomes (without drug) with laser treatment did not have any obvious effect in inhibiting tumor growth ($p = 0.165$). All of the mice from empty PoP liposomes with laser treatment, and saline control groups reached the 10 time tumor growth end point in ~2 weeks (0% survival rate). Taken together, Dox-PoP liposomes combined with laser treatment strongly inhibited tumor growth with synergy in the chemo- and photocomponents of the treatment. With laser treatment, Dox-CuPoP liposomes show comparable efficacy to Dox-PoP liposomes. The treatment was well tolerated, and there was less than 10% body weight loss (Figure 6B, 8.3% loss for Dox-CuPoP liposomes + laser group, 5.7% loss for Dox-PoP liposomes + laser group, 7.3% loss for empty PoP liposomes +laser group, 1.5% loss for Dox-PoP liposomes alone) 3 days following laser treatment. Mice continued to gain weight subsequently.

Histology and immunohistochemistry (IHC) were performed to examine molecular and microscopic aspects of the treatment (Figure 6C). Hematoxylin and eosin (HE) staining revealed that most tumor cells treated with Dox-CuPoP + laser lost their cell membrane and nucleus integrity, suggesting cellular necrosis. Dox-CuPoP + laser treatment also rapidly eliminated tumor cell proliferation as demonstrated by a lack of Ki67 IHC signal compared to the no laser treatment and saline control. Terminal deoxynucleotidyl transferase dUTP nick end labeling (TUNEL) staining further demonstrated that Dox-CuPoP with laser treatment induced apoptosis of virtually all cells in the laser treated tumor. Altogether, histological and IHC staining results were in agreement with the tumor growth study. CPT using Dox-CuPoP effectively inhibited cell proliferation and induced cell death, whereas the liposomes without phototreatment had little antitumor efficacy.

The microdistribution of Dox and PoP after laser treatment was investigated by fluorescence microscopy. Without laser treatment, liposomal Dox tended to localize near the tumor vasculature (Figure S4). After laser treatment, Dox appeared more diffuse in more spread out areas of the tumor tissue. This is likely due to the laser-induced release of Dox allowing for better Dox penetration since the free drug is able to traverse the tumor microenvironment better than the large liposomes.

Dox-CuPoP Accumulation in Lung Metastases. Lung metastases were established in mice 2 weeks after intravenous injection of 4T1 cells (20000 cells/mouse). The lungs of the mice were imaged *ex vivo* using bioluminescence to visualize

DOI: 10.1021/acsnano.7b06578
ACS Nano 2017, 11, 12482–12491

tumor metastasis and NIR fluorescence to visualize PoP (excitation 657 nm; emission 720 nm). Lungs were imaged 24 h following intravenous administration of Dox-CuPoP or Dox-PoP (5 mg/kg Dox) (Figure 7A,B). Fluorescence imaging showed that liposomes accumulated more (2.7- and 2.1-fold) in lungs with metastases compared to healthy lungs (Figure 7C). On the basis of tissue homogenates, Dox accumulation in lungs with metastases was higher (2.8- and 2.7-fold for Dox-CuPoP and Dox-PoP, respectively) than those in the healthy ones (Figure 7D). Similarly, PoP concentration in the lungs with metastasis was higher (2.88- and 2.0-fold for Dox-CuPoP and Dox-PoP, respectively) than in healthy lungs (Figure 7E). Additional optimization of liposome size and surface properties could potentially further reduce liposomal accumulation in healthy lungs.

Due to the enhanced permeabilization and retention (EPR) effect, liposomes are able to preferentially accumulate in tumors, which are characterized by leaky tumor vasculature.[50,51] To further investigate if Dox-CuPoP liposomes and Dox-PoP liposomes target to metastatic tumor nodules by EPR effect, frozen lung sections were prepared and imaged with fluorescence microscopy. Frozen luciferase-labeled tumors can be reimaged by direct addition of luciferin, Mg^{2+}, and ATP (Figure S5). The luciferase may still be active even if the tumor cells are not viable. Frozen section of the lungs were then produced, and luciferin, Mg^{2+}, and ATP were added to induce bioluminescence. The metastases in the lung could be identified and had some degree of colocalization with the PoP signal, demonstrating the metastasis-targeting potential of PoP-liposomes (Figure 8A). Moreover, the PoP signal in the lung with metastases were much stronger than that in the healthy lungs. This data is consistent with the PoP biodistribution in tumor-burdened lungs shown previously (Figure 7). Frozen sections of the lungs were then examined in confocal laser scanning microscopy (CLSM). The signal of PoP and Dox in the metastasis were higher than in the surrounding normal tissues and in the healthy lungs (Figure 8B). Moreover, Dox seemed to be already localized within the nuclei.

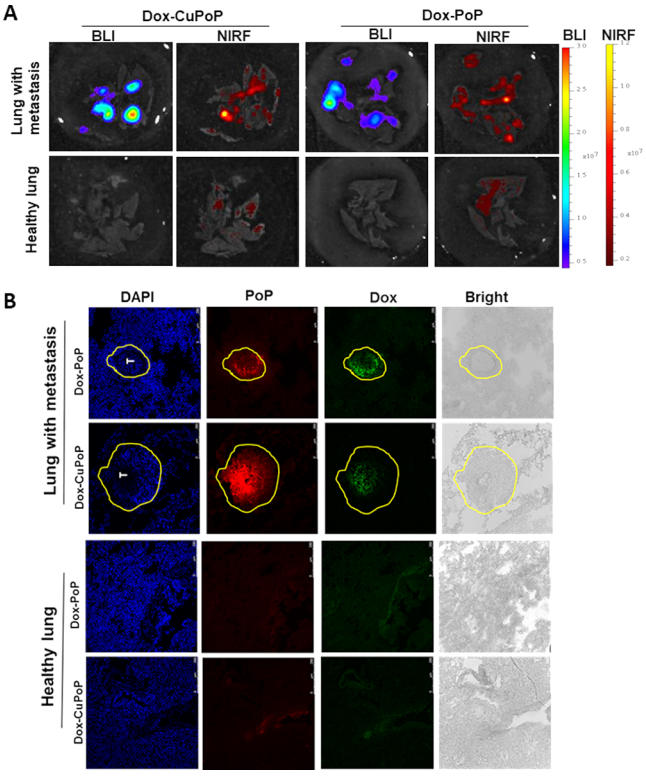

Figure 8. Frozen section imaging of Dox-CuPoP accumulation in 4T1 lung metastases. (A) Fluorescence imaging and luciferase imaging frozen lung sections. (B) Confocal laser scanning microscopy of lung sections.

CONCLUSION

We successfully developed a ^{64}Cu-labeling strategy for preformed, stealth Dox-PoP liposomes and demonstrated that the labeling process had minimal impact on liposome characteristics and function *in vitro* and *in vivo*. Both Dox-PoP liposomes and Dox-^{64}CuPoP liposomes effectively inhibited the growth of 4T1 orthotopic tumors when used in a single chemophototherapy treatment. ^{64}Cu-Dox-PoP liposomes could be used for PET and fluorescence imaging to identify the location of tumors and quantify liposome accumulation. Fluorescence imaging of ^{64}Cu-Dox-PoP liposomes could potentially be used for intraoperative guidance of light-delivery fibers for CPT. Dox-CuPoP accumulated in metastatic lung nodules. Thus, we conclude that PoP liposomes represent a liposomal construct with intrinsic imaging capabilities for IGDD and CPT.

MATERIALS AND METHODS

Liposome Preparation and Drug Loading. 1,2-Distearoyl-*sn*-glycero-3-phosphocholine (DSPC; no. LP-R4-076), cholesterol (no. CH-0355), 1,2-distearoylphosphatidylethanolamine methyl polyethylene glycol conjugate-2000 (DSPE-2000-PEG; no. LP-R4-039) were ordered from Corden Pharma. Porphyrin−phospholipid (PoP) used was *sn*-1-palmitoyl, *sn*-2-pyropheophorbide phosphtatidylcholine and was synthesized as previously reported.[18] PoP liposomes [DSPC/PoP/cholesterol/DSPE-2000-PEG], [53:2:40:5], mol % at the drug to lipid ratio of 1:6 were prepared by hot ethanol injection followed by high-pressure extrusion as previously described.[28,49] To generate 10 mL of PoP liposomes (20 mg/mL total lipids), lipids were first fully dissolved in 2 mL of hot ethanol (60 °C), followed by direct injection into 8 mL of 250 mM ammonium sulfate (pH 5.5) buffer at 60 °C. The lipid solution was fully mixed and passed 10 times at 60 °C through sequentially stacked polycarbonate membranes of 0.2, 0.1, and 0.08 μm pore size using a 10 mL LIPEX nitrogen pressurized extruder (Northern Lipids). Liposomes were then dialyzed with buffer containing 10% sucrose and 10 mM HEPES (pH 7.8) to remove free ammonium sulfate. Doxorubicin (LC Laboratories no. D-4000) was actively loaded into liposomes via ammonium sulfate gradient.[52] Drug was loaded by adding 20 mg/mL Dox solution to the liposomes at the drug to lipid ratio of 1:6 and incubated at 60 °C for 1 h.

^{64}Cu-Labeling. Copper-64 (^{64}Cu; $t_{1/2}$ = 12.7 h) was produced in an onsite GE PETrace cyclotron (University of Wisconsin—Madison) via the ^{64}Ni (p,n) ^{64}Cu reaction as reported previously.[53] For radiolabeling, 37 MBq of $^{64}CuCl_2$ was diluted in 300 μL of 0.1 M sodium acetate buffer (pH 5.5) and mixed with an aqueous solution of Dox-PoP liposomes (corresponding to 0.46 mg/mL PoP concentration). To enable intrinsic loading of ^{64}Cu into Dox-PoP liposomes, 1 vol % absolute ethanol was added to the mixture, followed by incubation at 37 °C for 4 h with constant shaking. The resulting Dox-^{64}CuPoP liposomes were purified by PD-10 size exclusion chromatography columns, using PBS as the mobile phase. Radiochemical yields were assessed by instant thin layer chromatography (TLC) using silica gel backed iTLC plates, with 50 mM EDTA solution as the running buffer. In order to demonstrate the role of PoP in intrinsic ^{64}Cu chelation, SSLD formulations (lacking PoP) were radiolabeled under the same experimental conditions to serve as control.

DOI: 10.1021/acsnano.7b06578
ACS Nano 2017, 11, 12482−12491

Liposome Characterization. Liposome size and polydisperisity were determined by dynamic light scattering via NanoBrook 90 Plus PALS in phosphate-buffered saline (PBS). Dox loading efficacy was determined by a spin column filtration method. Briefly, liposomes were diluted in 25 mM sodium chloride and placed in a 100 kDa cutoff spin column (Pall, no. OD100C34) and centrifuged at 2000*g* for 10 min. Unloaded Dox passed through the filter and was determined by UV spectroscopy. Serum stability was assessed by incubating PoP liposomes (0.1 mg/mL lipids) in 50% sterile bovine serum (Pel-Freeze) at 37 °C for 6 h. Total Dox fluorescence value was read after adding 0.25% Triton X-100 (Sigma, no. X100-500 ML). Dox release was calculated according to the formula $\%\text{Dox release} = \frac{F(\text{final}) - F(\text{initial})}{F(\text{TX}-100) - F(\text{initial})} \times 100$, where F (final), F(initial), and F(TX − 100) are Dox fluorescence before incubation, 6 h post incubation, and lysed with 0.25% Triton X-100, respectively. Light-triggered release rate was performed with a power-tunable 665 nm laser diode (RPMC Lasers, LDX-3115−665) at 100 or 250 mW/cm^2 as indicated. Dox fluorescence was recorded in real time during irradiation in a fluorometer (PTI). Before laser initiation, PoP liposomes (0.05 mg/mL) in 50% bovine serum were placed in a cuvette at 37 °C. 0.25% Triton X-100 was added after laser irradiation to read the final fluorescence. Dox release was assessed according to the above formula.

Fluorescence emission spectra were recorded for PoP and CuPoP liposomes following labeling by dissolving the liposomes in methanol. Equal concentrations of each sample were dissolved in methanol, and the emission spectra were recorded with an excitation of 400 nm using a PTI fluorometer. Singlet oxygen sensor green (SOSG, Life Technologies no. S-36002) was used for the detection of singlet oxygen generated by pyro-lipid during irradiation. SOSG fluorescence (exc./em. 504/525 nm) was recorded real time during irradiation in a fluometer (PTI). Light irradiation was performed in PBS containing SOSG and Dox-loaded PoP (PoP) liposomes.

Pharmacokinetics. Animal studies were carried out in accordance with the University at Buffalo, University of Wisconsin, and Shanghai Jiao Tong University School of Medicine IACUCs. Female CD-1 mice (18−20 g, Charles River) were intravenously injected visa tail vein with Dox-PoP liposomes or Dox-CuPoP liposomes at 7 mg/kg, n = 4. Small blood volumes were sampled from either submandibular and retroorbital locations at 0.5, 2, 4, 8, 24, and 48 h post injection. Blood was centrifuged at 1500*g* for 15 min. Serum was collected with a capillary collection tube (Microvette CB 300Z) and diluted in extraction buffer (0.075 N HCL, 90% isopropanol). Samples were then stored at −20 °C overnight followed by centrifugation at 10000*g* for 15 min. Supernatants were collected and analyzed by fluorescence in a 96 well plate reader. Dox was determined by a standard curve. Noncompartmental pharmacokinetics parameters were analyzed by PKsolver.

PET/Fluorescence Imaging and Biodistribution. Orthotopic 4T1 tumors were generated in 4−5 weeks old female BALB/c mice (Envigo, Indianapolis, IN) by injecting 1 × 10^6 4T1 murine breast cancer cells suspended in 30 μL PBS solution into the second mammary fat pad of the mouse. Tumors were monitored every other day, and mice were used typically 7−10 days after inoculation, when the tumor size reached 5−7 mm in diameter.

For *in vivo* PET/fluorescence imaging studies, 4T1 tumor-bearing mice (n = 3) were intravenously injected with 4−6 MBq of Dox-^{64}CuPoP liposomes (corresponding to a dose of 7 mg/kg Dox). Static PET scans were performed at 0.5, 3, 12, and 24 h postinjection on Inveon microPET/microCT rodent model scanner (Siemens Medical Solutions USA, Inc.), followed by fluorescence (FL) imaging on a PerkinElmer IVIS system, using 675/720 nm excitation/emission filters. PET Images were reconstructed using a maximum a posteriori (MAP) algorithm with no attenuation and scatter correction, and are presented as maximum intensity projections (MIP). 3D region-of-interest (ROI) analysis was performed on decay-corrected whole body images, using the vendor software (Inveon Research Workplace), and are presented as percentage of injected dose per gram (%ID/g). Quantitative PET data was then used to generate time-activity curves (TACs) for the tumor and other major organs of interest. FL image acquisition and 2D ROI analysis were carried out on vendor software (Living Image, PerkinElmer), and signal intensity within the ROIs is presented in the units of radiant efficiency ((p/s/cm^2/sr)/(μW/cm^2)).

Ex vivo biodistribution studies were performed after the final PET/FL scans at 24 h post injection to validate the *in vivo* findings. The mice (n = 3) were euthanized, and blood, tumor, and major organs were collected and wet-weighed. Radioactivity in each tissue was measured on a gamma counter (PerkinElmer) and presented as %ID/g. Extracted tumor and major organs were subjected to FL imaging using the excitation/emission filters 675/720 nm, followed by ROI analysis, as outlined previously.

Tumor Growth Inhibition in an Orthotopic Mouse Model. Five week old female nude mice (Jackson Laboratories, no. 007805) were inoculated with 2 × 10^4 4T1 cells. When tumor sizes reached 6−9 mm (initial tumor volumes 90−200 mm^3), mice were randomly grouped into five groups, six mice per group: (1) saline alone; (2) empty PoP liposomes + laser; (3) Dox-PoP liposomes without laser; (4) Dox-PoP liposomes with laser; (5) Cu labeled Dox-PoP liposomes with laser. A 200 μL portion of liposomal Dox (7 mg/kg Dox, 1.46 mg/kg PoP) or equivalent empty PoP liposomes (1.46 mg/kg PoP) was intravenously injected via tail vein. Laser irradiation were initiated 24 h post-injection for 33.3 min at 100 mW/cm2 (665 nm, 200 J/cm^2) while mice were anesthetized. Tumor volumes were calculated using the ellipsoid formula: volume $= \pi L\frac{W^2}{6}$, where L and W are the length and width of the tumor, respectively. Body weights of the mice were monitored for 3 weeks. Mice were sacrificed when tumor volumes exceeded 10 times of the initial volume or if tumors started to ulcerate (~20 days after laser treatment).

Histology and Immunohistochemistry. Formalin−fixed paraffin sections were cut at 4 μm. For H&E staining, slides were dewaxed through xylenes and graded alcohols, transferred to water for 3 min, hematoxylin for 3 min, water for 3 min, 1% acid alcohol for 1 min, water for 3 min, 0.2% ammonium hydroxide for 3 min, water for 4 min, 95% ethanol for 3 min, Eosin for 30 s, then dehydrated through graded alcohols, cleared, mounted, and coverslipped with xylene mount.

For Ki67 staining, slides were placed on charged slides and dried at 60 °C for 1 h. Slides were cooled to room temperature and added to the Dako Omnis autostainer, where they were deparaffinized with Clearify (American Mastertech; catalog no. CACLEGAL) and rinsed in water. Flex TRS Low (Dako; catalog no. GV805) was used for target retrieval for 30 min. Slides were incubated with Ki67 antibody (Thermo; catalog no. RM-9106-S1) for 20 min at 1/200 dilution. Rabbit Envision (Dako no. K4003) was applied for 30 min. DAB (diaminobenzidine) (Dako; catalog no. K3468) was applied for 5 min for visualization. Slides were counterstained with hematoxylin for 8 min then placed into water. After the slides were removed from the Omnis they were dehydrated, cleared, and coverslipped.

TUNEL staining was performed with a kit provided by EMD Millipore S7101. Slides were dewaxed through a series of xylenes and graded alcohols and then transferred to water. Slides were incubated in H_2O_2 for 10 min. Then Proteinase K was applied for 17 min followed by equilibration buffer while the TdT enzyme solution was being prepared. TdT enzyme solution was applied to slides for 75 min in a humidity chamber at 37°C. Slides were washed in stop/wash buffer for 10 min with agitation followed by antidigoxigenin−peroxidase for 30 min. DAB (diaminobenzidine) (Dako; catalog no. K3468) was applied for 3 min for visualization. Slides were counterstained with hematoxylin, dehydrated, cleared, and coverslipped.

Tumoral Drug Distribution by Fluorescence Microscopy. When 4T1 tumors reached ~10 mm, mice were placed into two groups (n = 3). Dox-CuPoP liposome (7 mg/kg) was intravenously administered. Twenty-four hours later, one group was irradiated with laser (100 mW/cm^2 for 33.3 min, 200 J/cm^2). Four hours post laser treatment, mice were sacrificed, and tumors were collected and fixed in 10% formalin for 24 h followed by submersion in 30% sucrose for 24 h. Tumors were embedded with OCT compound (VWR no. 25608-

DOI: 10.1021/acsnano.7b06578
ACS Nano 2017, 11, 12482−12491

930), snap frozen in liquid nitrogen, and stored at −80 °C prior to sectioning and fluorescence microscopy. Tumors were sectioned at 18 μm thickness. Fluorescence microscopy for Dox and PoP was carried out with a Nikon ECLIPSE fluorescence microscope with 20× objective lens. Dox was imaged with FITC channel, PoP was imaged with Texas Red channel, and Hoechst with DAPI channel.

Fluorescence Imaging on Lung Metastasis Mouse Model. The experimental lung metastasis model of murine mammary carcinoma 4T1 was established by intravenous injection of 2×10^5 luciferase-labeled 4T1 cells in 100 μL PBS into 6-week-old female BALB/c mice (Chinese Academy of Sciences, Shanghai, China). The bioluminescence signal in the chest region was assessed for metastasis every 3−4 days using the Xenogen IVIS 200 imaging system (Caliper Life Sciences).

Two weeks later, the mice with lung metastasis and healthy mice were injected with Dox-PoP and Dox-CuPoP liposomes via tail vein at a Dox dose of 5 mg/kg. After 24 h, the mice were intraperitoneally injected with firefly D-luciferin (150 mg/kg, J&K Chemical, Ltd.). Three minutes later, the mice were sacrificed and the lungs were *ex vivo* imaged to detect and/or quantify the bioluminescence signal for metastases and fluorescence for PoP (675 nm excitation; 720 nm emission). The lungs of the mice were then homogenized and analyzed for Dox and PoP contents using the fluorescence methods described previously.[28] Briefly, ∼100 mg of tissues was weighed and homogenized in 450 mL of nuclear lysis buffer [250 mM sucrose, 5 mM Tris−HCl, 1 mM $MgSO_4$,1 mM $CaCl_2$ (pH 7.6)] with a homogenizer. Homogenates (100 μL) were extracted with 900 μL of 0.075 N HCl 90% 2-propanol by mixing the samples and storage at −20 °C overnight. Samples were removed and centrifuged at 10000*g* for 15 min. The supernatant was collected, and the concentrations of Dox and PoP were determined fluorometrically.

Frozen Section Bioluminescence and Confocal Laser Scanning Microscopy. Bioluminescence is based on the oxidation of firefly luciferin by oxygen, catalyzed by luciferase. The oxidation reaction requires ATP and bivalent magnesium ions. The addition of exogenous ATP may trigger this reaction and light the tumor since the luciferase may still maintain its activity. To prove this hypothesis, a piece of mice thigh muscle and luciferase-labeled HT-29 colonic carcinoma tissue were coembedded in OCT and frozen at −80 °C overnight. Cryosections (50 μm) were then prepared on a cryostat (Leica CM1950, Wetzlar, Germany) for luciferase activity assay. The sections were overlaid with a substrate mix solution (firefly D-luciferin, 0.5 mg/mL; ATP, 1 mM in 0.01 M PBS containing bivalent magnesium ions), and imaged using the Xenogen IVIS 200 imaging system (Caliper Life Sciences) using the following parameters: exposure time = 1 s, FOV = 6.5, *f* = 1, binning = 4. The substrate mix solution without ATP was set as control, and the substrate mix solution alone was used as blank control.

Mice from the aforementioned lung metastasis study were sacrificed 24 h post drug administration, and lungs were resected for embedding, sectioning and bioluminescence imaging as described above. Then, *ex vivo* imaging of fluorescence was carried out with the parameters: 675 nm excitation, 720 nm emission, exposure time = 10 s, FOV = 6.5, f = 2, binning = 4. The distribution of liposomes in the lung was further analyzed using laser scanning confocal microscope (LSCM, Leica SP8). The embedded lung were cut into 10 μm section, washed 3 times with PBS and stabilized with 4% paraformaldehyde for 15 min. 4, 6-diamidino-2-phenylindole (DAPI) was used to stain nuclei. The distribution of PoP (633 nm excitation and 720 nm emission) and Dox (488 nm excitation and 590 nm emission) in the lung with metastasis was observed using LSCM.

ASSOCIATED CONTENT

Supporting Information

The Supporting Information is available free of charge on the ACS Publications website at DOI: 10.1021/acsnano.7b06578.

Figures S1−S5: ethanol-induced Dox leakage; morphology of Dox-PoP liposomes; laser-induced Dox release, singlet oxygen generation and quenching of PoP fluorescence; tumoral Dox microdistribution; frozen section luciferase reaction (PDF)

AUTHOR INFORMATION

Corresponding Authors

*E-mail: jflovell@buffalo.edu.
*E-mail: wcai@uwhealth.org.
*E-mail: fangchao32@sjtu.edu.cn.

ORCID

Weibo Cai: 0000-0003-4641-0833
Jonathan F. Lovell: 0000-0002-9052-884X

Notes

The authors declare no competing financial interest.

ACKNOWLEDGMENTS

This work was supported by the National Institutes of Health (R01EB017270, DP5OD017898, 1R01CA169365, P30CA014520, and UL1TR001412), the National Science Foundation (1555220), the University of Wisconsin—Madison, the American Cancer Society (125246-RSG-13-099-01-CCE), and the National Natural Science Foundation of China (81572998 and 81773274). We acknowledge assistance from the National Cancer Institute Nanotechnology Characterization Laboratory for cyro-electron micrographs.

REFERENCES

(1) Lammers, T.; Kiessling, F.; Hennink, W.; Storm, G. Nanotheranostics and image-guided drug delivery: current concepts and future directions. *Mol. Pharmaceutics* **2010**, *7*, 1899−1912.

(2) Guo, C.; Jin, Y.; Dai, Z. Multifunctional Ultrasound Contrast Agents for Imaging Guided Photothermal Therapy. *Bioconjugate Chem.* **2014**, *25*, 840−854.

(3) Janib, S. M.; Moses, A. S.; MacKay, J. A. Imaging and Drug Delivery Using Theranostic Nanoparticles. *Adv. Drug Delivery Rev.* **2010**, *62*, 1052−1063.

(4) Bao, G.; Mitragotri, S.; Tong, S. Multifunctional Nanoparticles for Drug Delivery and Molecular Imaging. *Annu. Rev. Biomed. Eng.* **2013**, *15*, 253−282.

(5) Fernandez-Fernandez, A.; Manchanda, R.; McGoron, A. J. Theranostic Applications of Nanomaterials in Cancer: Drug Delivery, Image-Guided Therapy, and Multifunctional Platforms. *Appl. Biochem. Biotechnol.* **2011**, *165*, 1628−1651.

(6) Yang, G.; Gong, H.; Liu, T.; Sun, X.; Cheng, L.; Liu, Z. Two-dimensional Magnetic WS2@Fe3O4 Nanocomposite with Mesoporous Silica Coating for Drug Delivery and Imaging-Guided Therapy of Cancer. *Biomaterials* **2015**, *60*, 62−71.

(7) Kim, D.; Jeong, Y. Y.; Jon, S. A Drug-Loaded Aptamer−Gold Nanoparticle Bioconjugate for Combined CT Imaging and Therapy of Prostate Cancer. *ACS Nano* **2010**, *4*, 3689−3696.

(8) Chen, Y.; Ai, K.; Liu, J.; Sun, G.; Yin, Q.; Lu, L. Multifunctional Envelope-Type Mesoporous Silica Nanoparticles for pH-Responsive Drug Delivery and Magnetic Resonance Imaging. *Biomaterials* **2015**, *60*, 111−120.

(9) Shen, J.; Zhao, L.; Han, G. Lanthanide-Doped Upconverting Luminescent Nanoparticle Platforms for Optical Imaging-Guided Drug Delivery and Therapy. *Adv. Drug Delivery Rev.* **2013**, *65*, 744−755.

(10) Jiang, Y.; Cui, D.; Fang, Y.; Zhen, X.; Upputuri, P.; Pramanik, M.; Ding, D.; Pu, K. Amphiphilic Semiconducting Polymer as Multifunctional Nanocarrier for Fluorescence/Photoacoustic Imaging Guided Chemo-Photothermal Therapy. *Biomaterials* **2017**, *145*, 168.

(11) Jiang, Y.; Pu, K. Advanced Photoacoustic Imaging Applications of Near-Infrared Absorbing Organic Nanoparticles. *Small* **2017**, *13*, 1700710.

DOI: 10.1021/acsnano.7b06578
ACS Nano 2017, 11, 12482−12491

(12) Lyu, Y.; Zhen, X.; Miao, Y.; Pu, K. Reaction-Based Semiconducting Polymer Nanoprobes for Photoacoustic Imaging of Protein Sulfenic Acids. *ACS Nano* **2017**, *11*, 358−367.
(13) Huang, H.; Lovell, J. F. Advanced Functional Nanomaterials for Theranostics. *Adv. Funct. Mater.* **2017**, *27*, 1603524.
(14) Feng, L.; Gao, M.; Tao, D.; Chen, Q.; Wang, H.; Dong, Z.; Chen, M.; Liu, Z. Cisplatin-Prodrug-Constructed Liposomes as a Versatile Theranostic Nanoplatform for Bimodal Imaging Guided Combination Cancer Therapy. *Adv. Funct. Mater.* **2016**, *26*, 2207−2217.
(15) Jing, L.; Shi, J.; Fan, D.; Li, Y.; Liu, R.; Dai, Z.; Wang, F.; Tian, J. 177Lu-Labeled Cerasomes Encapsulating Indocyanine Green for Cancer Theranostics. *ACS Appl. Mater. Interfaces* **2015**, *7*, 22095−22105.
(16) Feng, L.; Cheng, L.; Dong, Z.; Tao, D.; Barnhart, T. E.; Cai, W.; Chen, M.; Liu, Z. Theranostic Liposomes with Hypoxia-Activated Prodrug to Effectively Destruct Hypoxic Tumors Post-Photodynamic Therapy. *ACS Nano* **2017**, *11*, 927−937.
(17) Ponce, A.; Viglianti, B.; Yu, D.; Yarmolenko, P.; Michelich, C.; Woo, J.; Bally, M.; Dewhirst, M. Magnetic Resonance Imaging of Temperature-Sensitive Liposome Release: Drug Dose Painting and Antitumor Effects. *J. Nat. Cancer Inst.* **2007**, *99*, 53−63.
(18) Carter, K. A.; Shao, S.; Hoopes, M. I.; Luo, D.; Ahsan, B.; Grigoryants, V. M.; Song, W.; Huang, H.; Zhang, G.; Pandey, R. K.; Geng, J.; Pfeifer, B. A.; Scholes, C. P.; Ortega, J.; Karttunen, M.; Lovell, J. F. Porphyrin-Phospholipid Liposomes Permeabilized by Near-Infrared Light. *Nat. Commun.* **2014**, *5*, 3546.
(19) Luo, D.; Carter, K. A.; Miranda, D.; Lovell, J. F. Chemophototherapy: An Emerging Treatment Option for Solid Tumors. *Adv. Sci.* **2017**, *4*, 1600106.
(20) Luo, D.; Geng, J.; Li, N.; Carter, K.; Shao, S.; Atilla-Gokcumen, G.; Lovell, J. Vessel-Targeted Chemophototherapy with Cationic Porphyrin-Phospholipid Liposomes. *Mol. Cancer Ther.* **2017**, *16*, 2452−2461.
(21) Weissleder, R. Molecular Imaging in Cancer. *Science* **2006**, *312*, 1168−1171.
(22) Shafirstein, G.; Bellnier, D.; Oakley, E.; Hamilton, S.; Potasek, M.; Beeson, K.; Parilov, E. Interstitial Photodynamic Therapy—A Focused Review. *Cancers* **2017**, *9*, 12.
(23) Andresen, T. L.; Jensen, S. S.; Jørgensen, K. Advanced Strategies in Liposomal Cancer Therapy: Problems and Prospects of Active and Tumor Specific Drug Release. *Prog. Lipid Res.* **2005**, *44*, 68−97.
(24) Lu, Y.; Aimetti, A. A.; Langer, R.; Gu, Z. Bioresponsive Materials. *Nat. Rev. Mater.* **2016**, *2*, 16075.
(25) Spring, B. Q.; Sears, R. B.; Zheng, L. Z.; Mai, Z.; Watanabe, R.; Sherwood, M. E.; Schoenfeld, D. A.; Pogue, B. W.; Pereira, S. P.; Villa, E.; Hasan, T. A Photoactivable Multi-Inhibitor Nanoliposome for Tumour Control and Simultaneous Inhibition of Treatment Escape Pathways. *Nat. Nanotechnol.* **2016**, *11*, 378−387.
(26) Miranda, D.; Lovell, J. F. Mechanisms of Light-Induced Liposome Permeabilization. *Bioeng. Trans. Med.* **2016**, *1*, 267−276.
(27) Rwei, A. Y.; Lee, J.-J.; Zhan, C.; Liu, Q.; Ok, M. T.; Shankarappa, S. A.; Langer, R.; Kohane, D. S. Repeatable and Adjustable On-Demand Sciatic Nerve Block with Phototriggerable Liposomes. *Proc. Natl. Acad. Sci. U. S. A.* **2015**, *112*, 15719−15724.
(28) Luo, D.; Carter, K.; Razi, A.; Geng, J.; Shao, S.; Giraldo, D.; Sunar, U.; Ortega, J.; Lovell, J. Doxorubicin Encapsulated In Stealth Liposomes Conferred with Light-Triggered Drug Release. *Biomaterials* **2016**, *75*, 193−202.
(29) Allen, T. M.; Cullis, P. R. Liposomal Drug Delivery Systems: From Concept to Clinical Applications. *Adv. Drug Delivery Rev.* **2013**, *65*, 36−48.
(30) O'Brien, M. E. R.; Wigler, N.; Inbar, M.; Rosso, R.; Grischke, E.; Santoro, A.; Catane, R.; Kieback, D. G.; Tomczak, P.; Ackland, S. P.; Orlandi, F.; Mellars, L.; Alland, L.; Tendler, C. Reduced Cardiotoxicity and Comparable Efficacy in a Phase III Trial of Pegylated Liposomal Doxorubicin HCl (CAELYX/Doxil®) *versus* Conventional Doxorubicin for First-Line Treatment of Metastatic Breast Cancer. *Ann. Oncol.* **2004**, *15*, 440−449.
(31) Harrington, K. J.; Mohammadtaghi, S.; Uster, P. S.; Glass, D.; Peters, A. M.; Vile, R. G.; Stewart, J. S. W. Effective Targeting of Solid Tumors in Patients With Locally Advanced Cancers by Radiolabeled Pegylated Liposomes. *Clin. Cancer Res.* **2001**, *7*, 243−254.
(32) Sun, X.; Huang, X.; Yan, X.; Wang, Y.; Guo, J.; Jacobson, O.; Liu, D.; Szajek, L. P.; Zhu, W.; Niu, G.; Kiesewetter, D. O.; Sun, S.; Chen, X. Chelator-Free 64Cu-Integrated Gold Nanomaterials for Positron Emission Tomography Imaging Guided Photothermal Cancer Therapy. *ACS Nano* **2014**, *8*, 8438−8446.
(33) Guo, W.; Sun, X.; Jacobson, O.; Yan, X.; Min, K.; Srivatsan, A.; Niu, G.; Kiesewetter, D. O.; Chang, J.; Chen, X. Intrinsically Radioactive [64Cu]CuInS/ZnS Quantum Dots for PET and Optical Imaging: Improved Radiochemical Stability and Controllable Cerenkov Luminescence. *ACS Nano* **2015**, *9*, 488−495.
(34) Pang, B.; Zhao, Y.; Luehmann, H.; Yang, X.; Detering, L.; You, M.; Zhang, C.; Zhang, L.; Li, Z.-Y.; Ren, Q.; Liu, Y.; Xia, Y. 64Cu-Doped PdCu@Au Tripods: A Multifunctional Nanomaterial for Positron Emission Tomography and Image-Guided Photothermal Cancer Treatment. *ACS Nano* **2016**, *10*, 3121−3131.
(35) Gao, F.; Cai, P.; Yang, W.; Xue, J.; Gao, L.; Liu, R.; Wang, Y.; Zhao, Y.; He, X.; Zhao, L.; Huang, G.; Wu, F.; Zhao, Y.; Chai, Z.; Gao, X. Ultrasmall [64Cu]Cu Nanoclusters for Targeting Orthotopic Lung Tumors Using Accurate Positron Emission Tomography Imaging. *ACS Nano* **2015**, *9*, 4976−4986.
(36) Shen, S.; Jiang, D.; Cheng, L.; Chao, Y.; Nie, K.; Dong, Z.; Kutyreff, C. J.; Engle, J. W.; Huang, P.; Cai, W.; Liu, Z. Renal-Clearable Ultrasmall Coordination Polymer Nanodots for Chelator-Free 64Cu-Labeling and Imaging-Guided Enhanced Radiotherapy of Cancer. *ACS Nano* **2017**, *11*, 9103−9111.
(37) Petersen, A.; Binderup, T.; Rasmussen, P.; Henriksen, J.; Elema, D.; Kjær, A.; Andresen, T. 64Cu loaded liposomes as positron emission tomography imaging agents. *Biomaterials* **2011**, *32*, 2334−2341.
(38) Hansen, A.; Petersen, A.; Henriksen, J.; Boerresen, B.; Rasmussen, P.; Elema, D.; Rosenschöld, P.; Kristensen, A.; Kjær, A.; Andresen, T. Positron Emission Tomography Based Elucidation of the Enhanced Permeability and Retention Effect in Dogs with Cancer Using Copper-64 Liposomes. *ACS Nano* **2015**, *9*, 6985−6995.
(39) Edmonds, S.; Volpe, A.; Shmeeda, H.; Parente-Pereira, A. C.; Radia, R.; Baguña-Torres, J.; Szanda, I.; Severin, G. W.; Livieratos, L.; Blower, P. J.; Maher, J.; Fruhwirth, G. O.; Gabizon, A.; T. M. de Rosales, R. Exploiting the Metal-Chelating Properties of the Drug Cargo for In Vivo Positron Emission Tomography Imaging of Liposomal Nanomedicines. *ACS Nano* **2016**, *10*, 10294−10307.
(40) Carter, K.; Wang, S.; Geng, J.; Luo, D.; Shao, S.; Lovell, J. Metal Chelation Modulates Phototherapeutic Properties of Mitoxantrone-Loaded Porphyrin-Phospholipid Liposomes. *Mol. Pharmaceutics* **2016**, *13*, 420−427.
(41) Rieffel, J.; Chen, F.; Kim, J.; Chen, G.; Shao, W.; Shao, S.; Chitgupi, U.; Hernandez, R.; Graves, S. A.; Nickles, R. J.; Prasad, P. N.; Kim, C.; Cai, W.; Lovell, J. F. Hexamodal Imaging with Porphyrin-Phospholipid-Coated Upconversion Nanoparticles. *Adv. Mater.* **2015**, *27*, 1785−1790.
(42) Lovell, J. F.; Jin, C. S.; Huynh, E.; Jin, H.; Kim, C.; Rubinstein, J. L.; Chan, W. C. W.; Cao, W.; Wang, L. V.; Zheng, G. Porphysome Nanovesicles Generated by Porphyrin Bilayers for Use as Multimodal Biophotonic Contrast Agents. *Nat. Mater.* **2011**, *10*, 324−332.
(43) Shao, S.; Geng, J.; Ah Yi, H.; Gogia, S.; Neelamegham, S.; Jacobs, A.; Lovell, J. F. Functionalization of Cobalt Porphyrin-Phospholipid Bilayers with His-Tagged Ligands and Antigens. *Nat. Chem.* **2015**, *7*, 438−446.
(44) Muhanna, N.; Cui, L.; Chan, H.; Burgess, L.; Jin, C. S.; MacDonald, T. D.; Huynh, E.; Wang, F.; Chen, J.; Irish, J. C.; Zheng, G. Multimodal Image-Guided Surgical and Photodynamic Interventions in Head and Neck Cancer: From Primary Tumor to Metastatic Drainage. *Clin. Cancer Res.* **2016**, *22*, 961−970.
(45) Liu, T. W.; MacDonald, T. D.; Shi, J.; Wilson, B. C.; Zheng, G. Intrinsically Copper-64-Labeled Organic Nanoparticles as Radiotracers. *Angew. Chem., Int. Ed.* **2012**, *51*, 13128−13131.

DOI: 10.1021/acsnano.7b06578
ACS Nano 2017, 11, 12482−12491

(46) Shao, S.; Do, T. N.; Razi, A.; Chitgupi, U.; Geng, J.; Alsop, R. J.; Dzikovski, B. G.; Rheinstädter, M. C.; Ortega, J.; Karttunen, M.; Spernyak, J. A.; Lovell, J. F. Design of Hydrated Porphyrin-Phospholipid Bilayers with Enhanced Magnetic Resonance Contrast. *Small* **2017**, *13*, 1602505.
(47) Barry, J. A.; Gawrisch, K. Direct NMR evidence for Ethanol Binding to the Lipid-Water Interface of Phospholipid Bilayers. *Biochemistry* **1994**, *33*, 8082−8088.
(48) Miranda, D.; Carter, K.; Luo, D.; Shao, S.; Geng, J.; Li, C.; Chitgupi, U.; Turowski, S. G.; Li, N.; Atilla-Gokcumen, G. E.; Spernyak, J. A.; Lovell, J. F. Multifunctional Liposomes for Image-Guided Intratumoral Chemo-Phototherapy. *Adv. Healthcare Mater.* **2017**, *6*, 1700253.
(49) Luo, D.; Li, N.; Carter, K. A.; Lin, C.; Geng, J.; Shao, S.; Huang, W. C.; Qin, Y.; Atilla-Gokcumen, G. E.; Lovell, J. F. Rapid Light-Triggered Drug Release in Liposomes Containing Small Amounts of Unsaturated and Porphyrin-Phospholipids. *Small* **2016**, *12*, 3039−3047.
(50) Iyer, A. K.; Khaled, G.; Fang, J.; Maeda, H. Exploiting the Enhanced Permeability and Retention Effect for Tumor Targeting. Drug Discov. *Drug Discovery Today* **2006**, *11*, 812−818.
(51) Yuan, F.; Leunig, M.; Huang, S.; Berk, D.; Papahadjopoulos, D.; Jain, R. Microvascular Permeability and Interstitial Penetration of Sterically Stabilized (Stealth) Liposomes in a Human Tumor Xenograft. *Cancer Res.* **1994**, *54*, 3352−3356.
(52) Haran, G.; Cohen, R.; Bar, L.; Barenholz, Y. Transmembrane Ammonium Sulfate Gradients In Liposomes Produce Efficient and Stable Entrapment of Amphipathic Weak Bases. *Biochim. Biophys. Acta, Biomembr.* **1993**, *1151*, 201−215.
(53) Hong, H.; Zhang, Y.; Orbay, H.; Valdovinos, H. F.; Nayak, T. R.; Bean, J.; Theuer, C. P.; Barnhart, T. E.; Cai, W. Positron Emission Tomography Imaging of Tumor Angiogenesis with a (61/64)Cu-Labeled F(Ab')(2) Antibody Fragment. *Mol. Pharmaceutics* **2013**, *10*, 709−716.

DOI: 10.1021/acsnano.7b06578
ACS Nano 2017, 11, 12482−12491